Electronic Supplementary Material (ESI) for Soft Matter.

Supplementary Information for Assembly of nothing: Equilibrium fluids with designed structured porosity

Beth A. Lindquist, Ryan B. Jadrich, and Thomas M. Truskett*

McKetta Department of Chemical Engineering, University of Texas at Austin, Austin, TX 78712

E-mail: truskett@che.utexas.edu

*To whom correspondence should be addressed

Computational Methods

Simulation and Analysis Details

To calculate $g_{\rm tgt}(r)$, we simulated $N = 5475$ small (S) particles in a frozen matrix of 32 large (L) template spheres to create pores. Small particles are excluded from one another and from large particles via effective hard core repulsions of diameter σ and cross diameter 2.5σ, respectively. The packing fraction $\eta = \pi\sigma^3 N/6V$ of the small spheres in volume V is 0.31. Simulations were performed using the GROMACS 4.6.5 molecular dynamics package[1,2] with the 50-25 Weeks-Chandler-Andersen (WCA) effective hardcore potential[3]

$$u_{\rm WCA}^{(i,j)}(r) \equiv H(2^{1/25}\sigma_{i,j} - r)\left(4\epsilon\left[\left(\frac{\sigma_{i,j}}{r}\right)^{50} - \left(\frac{\sigma_{i,j}}{r}\right)^{25}\right] + \epsilon\right) \tag{1}$$

where $\sigma_{S,S} = \sigma$, $\sigma_{S,L} = 2.5\sigma$ and $H(x)$ is the Heaviside step function. In standard GROMACS units (see GROMACS manual) we set $\sigma = 1$, $\epsilon = 1.0$, $m = 30$ (mass), $dt = 0.001$ (time step) and $T = 300$ via velocity-rescale thermostating with characteristic time constant $\tau = 100dt$ and rescaling every $10dt$. These conditions yield the dimensionless relations $\beta\epsilon \approx 0.4$ for the WCA potential and $dt/t_0 \approx 0.0003$ where $t_0 \equiv \sqrt{\sigma^2 m/(k_B T)}$ is the elementary ballistic time of the molecular dynamics simulation. The choice $\beta\epsilon$ is not unique; it served only to furnish a steep repulsion mimicking a hardcore–even a totally different functional form that is sufficiently steep would suffice. With this, a target RDF with pores of a prescribed size was generated for the inverse design (ID) step. (Note: in practice, the ID step employs a fixed simulation temperature; however, this is totally arbitrary, and variation would lead to trivial rescaling of the optimized potential such that its thermally non-dimensionalized form is unique).

To check for finite size effects, simulations of all optimized potentials were performed with 18478 particles, which corresponds to increasing the box size used in the ID optimization by a factor of 1.5. Starting from a disordered configuration, a lattice of pores is typically

formed within $\approx 1,000,000 dt/t_0 = 300$ short time non-dimensionalized units–a relatively short timescale for molecular dynamics simulations. As a zeroth order comparison to a system with solvent, we assume our molecular dynamics ballistic short time unit can be replaced by a short time diffusion scale in a solvent based system. (This also neglects possible complications from hydrodynamic effects.) For $25nm$, $100nm$ and $2\mu m$ particles in common solvents, the estimates for t_0 are 0.15ms, 0.01s and 30s, respectively.[4] Thus, the corresponding times to assembly under our very simplified assumptions are 0.045s, 3s and 150min. While these estimates may seem rather fast, they provide a rough estimate of the expected order for the time to assembly.

As described in the main text, pores were characterized via insertion of spheres with a diameter of 2σ such that they did not overlap with the system particles. The pore volumes were determined via Monte Carlo integration of the inserted void particles, where the inserted spheres were assigned to a given pore based on a clustering analysis, where overlapping spheres are taken to be neighbors.[5] The resulting volume is then converted to the diameter of a sphere of equal volume. This strategy allows for an evaluation of moderately aspherical pores. Though visual inspection reveals that the pores are relatively spherical, instantaneous fluctuations of the pore walls as well as infrequent particle motions through the pores render the assumption of perfectly spherical pores (often employed in the calculation of pore size distributions) inaccurate for this case, under-predicting the pore size.

As discussed in the main text, the target simulation was chosen such that the pore diameter was similar to the thickness of pore "walls" to find a target well suited to a description with a pair potential: the large particles were fixed on an FCC lattice with a nearest neighbor distance of 7.4σ. We also tried an optimization with a template composed of frozen disordered large particles, the positions of which were generated from a simulation of only the large particles with effective hard core repulsions of diameter 6σ. All other parameters were identical to those described above. (In the binary target simulation, the large particles still interacted with the small particles via a 4σ effective hard core.) We performed 10

target simulations, each using a different simulation snapshot for the template, and found that $g_{\mathrm{tgt}}(r)$ was essentially invariant with respect to the different frozen templates. We then performed the IBI optimization with the $g_{\mathrm{tgt}}(r)$ that was averaged over the different frozen templates. Despite the larger mismatch between pore diameter and pore wall size, this potential still yielded discrete pores, positioned on a defective FCC lattice where the pores have significantly more translational motion about their lattice sites. However, the pores are somewhat smaller and thus do not reproduce the targeted pore size as well (the maximum in the pore size distribution function is $\approx 3.6\sigma$). Therefore, while there is a range of acceptable templates that can form pores, a target system with a matching pore wall thickness and pore diameter seems to be more accurately reproduced by a pair potential.

Inverse Design Methodology

Unconstrained potential optimizations were performed using iterative Boltzmann inversion (IBI), a powerful inverse statistical mechanics tool from the coarse-graining community.[6] IBI assumes nothing about the functional form of the potential and seeks to exactly replicate $g_{\mathrm{tgt}}(r)$. In practice, the potential is finely discretized, cut and shifted at a finite cutoff distance (R_{C}), and spline fitted. In a preliminary IBI optimization, R_{C} was set equal to one-half of the box length (10.5σ). This potential, shown in Fig. S1, formed pores on an FCC lattice; however, when the potential was simulated in a larger box, the system phase separated into a liquid and a gas (though a metastable porous phase was observed en route to macrophase separation). Suspecting that the long-range attraction was responsible for these finite-size effects, and noting from our earlier work that only a single attractive well and repulsive hump were needed to form clusters,[7] we cut and shifted the potential at the minimum at 7.3σ. We then re-optimized the potential with $R_{\mathrm{C}} = 7.3\sigma$ to yield the final IBI potential. The behavior of the resulting potential was robust with respect to increasing the box size. IBI calculations were performed using the the Versatile Object-oriented Toolkit for Coarse-graining Applications (VOTCA),[8,9] which interfaces with the GROMACS 4.6.5

molecular dynamics (MD) package.[1,2]

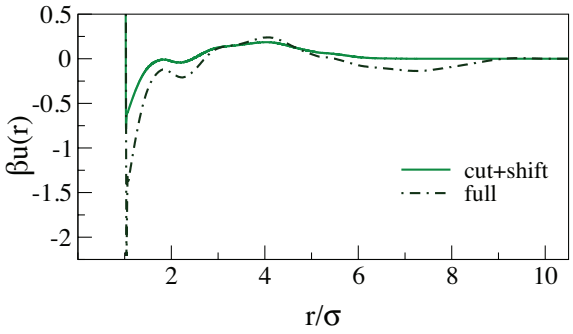

Figure S1: IBI-optimized potentials with $R_{\rm C} = 10.5\sigma$ and 7.3σ.

For optimizing constrained analytical forms, we utilized Relative Entropy (RE) optimization.[6,10,11] Two functional forms (denoted by the roman numeral indices I and II) for the interactions external to the WCA core are considered

$$u^{(i)}_{\rm RE}(r) \equiv -\epsilon_1 \exp\left[-\left(\frac{r-d-\alpha_1/2}{\alpha_1/2}\right)^{n_1}\right] + \epsilon_2 q_i(\alpha_1,\alpha_2)\exp\left[-\left(\frac{r-d-\alpha_2/2-\alpha_1}{\alpha_2/2}\right)^{n_2}\right] \quad (2)$$

where

$$q_i(\alpha_1,\alpha_2) \equiv \delta_{i,\rm I} + \delta_{i,\rm II}\left[\frac{-r+d+\alpha_1+\alpha_2}{\alpha_2}\right] \quad (3)$$

$\delta_{i,j}$ is the Kronecker delta, $[\epsilon_1, \epsilon_2]$ are the [attractive, repulsive] strengths, and $[\alpha_1, \alpha_2]$ are the corresponding ranges. The term for the type II potential effectively changes the symmetric repulsive hump to a linear ramp. Two exponents also appear, $[n_1, n_2]$ which we set to various numbers to test the flexibility of such potentials to make pores. We use the compact notation, $i{\rm A}n_1{\rm R}n_2$, to denote the type and the exponents as in Figure 4a of the main text. Attraction strengths and ranges are then optimized within the relative entropy framework by maximizing the log-likelihood of sampling the target configurations using a simple gradient descent scheme.[12] Optimized parameters are provided in Table S1.

Table S1. Optimal parameters for the constrained potentials.

Type	n_1	n_2	$\beta\epsilon_1$	α_1	$\beta\epsilon_2$	α_2
I	4	2	0.215	1.46	0.218	2.55
I	8	8	0.187	1.46	0.183	2.56
II	6	6	0.353	1.54	0.322	2.72

Cluster Size Distributions

Cluster size distributions (CSDs)[5] for the clustered phase as a function of density are shown in Fig. S2. The CSDs are somewhat sensitive to the choice of distance cutoff, R_{CSD}, used to determine whether particles are neighbors, though the overall trends remain the same regardless of R_{CSD}. The relatively broad attractive well in the potential (Fig. S1) makes determination of R_{CSD} non-unique; therefore, a value of $R_{\mathrm{CSD}} = 1.33\sigma$ was chosen such that two discrete clusters were assigned to a single cluster over an order of magnitude less frequently than a single cluster was identified; these dimers are not shown in Fig. S2 for clarity. Fig. S2 indicates that, while there is a significant fraction of monomer present, the clusters are reasonably size specific, particularly at the higher densities where there is essentially perfect separation of monomer/small aggregates and clusters. As η is further decreased, the clusters break up and become less size specific, until at approximately $\eta < 0.04$ there is no shoulder in the CSD, indicating no preferred size scale for clustering.

In our prior work,[7] we used IBI to discover potentials which generated a dilute fluid of clusters. By contrast, the clusters in the present study appear on lattice positions as can be seen in Fig. 3 of the main text. Moreover, we visually observe greater particle exchange among the clusters in the current work, as well as a greater fraction of monomer in the CSDs. Both of these observations are in keeping with the shorter (though broader) repulsive hump seen in the pore-forming potentials. In prior work, due to the additive effects of the relatively sharp and tall repulsive humps of the constituent particles, each cluster acted essentially as a re-normalized object, and so the CSDs were only subtly sensitive to changes in density. Here however, the cluster size is much more responsive to changes in overall density.

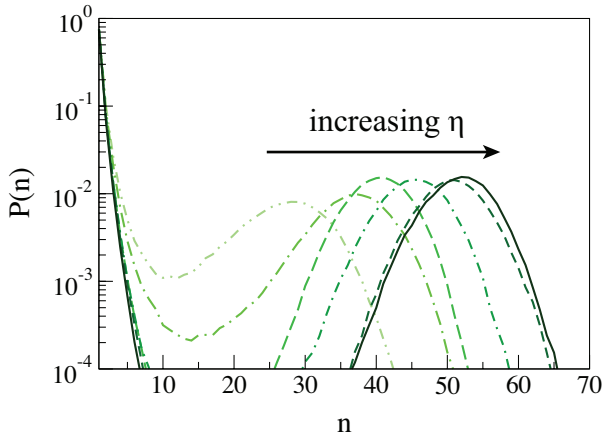

Figure S2: CSDs for $\eta = 0.052$ to 0.082 in increments of 0.006.

Visualization of the Relative Entropy Potential Simulations

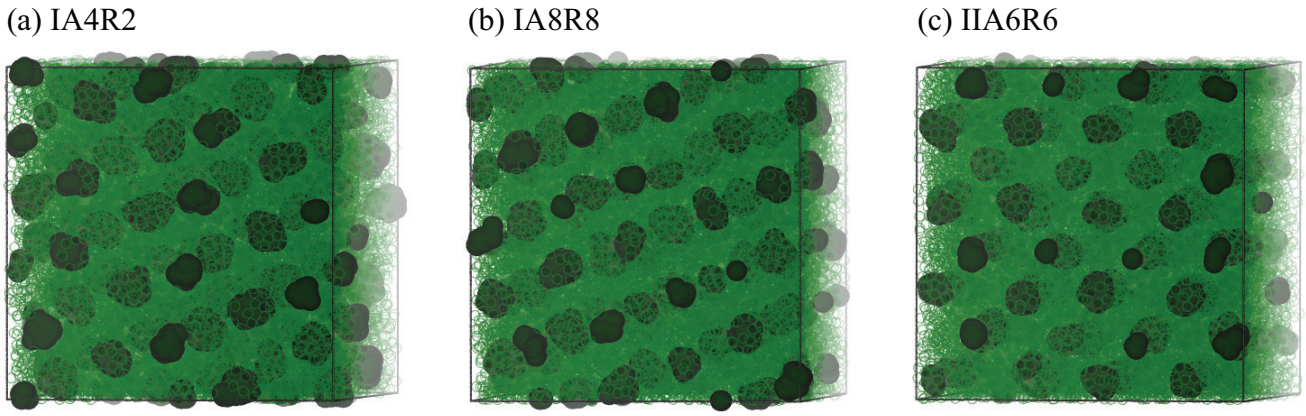

Figure S3: A visualization of the particles and void space as in Fig. 1c of the main text, where the former are lighter green and transparent and the latter is darker and opaque. Ordered, discrete pores are observed in all cases.

References

(1) Van Der Spoel, D.; Lindahl, E.; Hess, B.; Groenhof, G.; Mark, A. E.; Berendsen, H. J. C. GROMACS: Fast, flexible, and free. *J. Comput. Chem.* **2005**, *26*, 1701–1718.

(2) Plimpton, S. Fast Parallel Algorithms for Short-Range Molecular Dynamics. *J. Comput. Phys.* **1995**, *117*, 1–19.

(3) Hansen, J.-P.; McDonald, I. R. *Theory of Simple Liquids*, 3rd ed.; Academic Press: New York, NY, USA, 2006.

(4) Jadrich, R.; Schweizer, K. S. Percolation, phase separation, and gelation in fluids and mixtures of spheres and rods. *The Journal of Chemical Physics* **2011**, *135*, 234902.

(5) Godfrin, P. D.; Valadez-Perez, N. E.; Castaneda-Priego, R.; Wagner, N. J.; Liu, Y. Generalized phase behavior of cluster formation in colloidal dispersions with competing interactions. *Soft Matter* **2014**, *10*, 5061–5071.

(6) Noid, W. G. Perspective: Coarse-grained models for biomolecular systems. *J. Chem. Phys.* **2013**, *139*, 090901.

(7) Jadrich, R. B.; Bollinger, J. A.; Lindquist, B. A.; Truskett, T. M. Equilibrium cluster fluids: pair interactions via inverse design. *Soft Matter* **2015**, 9342–9354.

(8) Rühle, V.; Junghans, C.; Lukyanov, A.; Kremer, K.; Andrienko, D. Versatile Object-Oriented Toolkit for Coarse-Graining Applications. *J. Chem. Theory Comput.* **2009**, *5*, 3211–3223.

(9) Mashayak, S. Y.; Jochum, M. N.; Koschke, K.; Aluru, N. R.; Rühle, V.; Junghans, C. Relative Entropy and Optimization-Driven Coarse-Graining Methods in VOTCA. *PLoS ONE* **2015**, *10*, e0131754.

(10) Chaimovich, A.; Shell, M. S. Coarse-graining errors and numerical optimization using a relative entropy framework. *J. Chem. Phys.* **2011**, *134*, 094112.

(11) Fu, C.-C.; Kulkarni, P. M.; Shell, M. S.; Gary Leal, L. A test of systematic coarse-graining of molecular dynamics simulations: Thermodynamic properties. *J. Chem. Phys.* **2012**, *137*, 164106.

(12) Barber, D. *Bayesian Reasoning and Machine Learning*; Cambridge University Press, 2012.